

CHAPTER 202

A NUMERICAL MODEL FOR SAND TRANSPORT UNDER COMPOUND WAVES

Shinji Sato

Associate Professor, Civil Eng. Dept., Yokohama National Univ.
Tokiwadai, Hodogaya-ku, Yokohama 240, JAPAN

Norihiko Mitsunobu

Shizuoka Prefectural Government

1. INTRODUCTION

In order to understand sediment transport around various maritime structures, it is essential to elucidate the mechanism of sand transport under compound waves. Although numerous studies have been carried out on sand transport, most of them have been concentrated to the sand movement mechanism under one-component wave. Laboratory experiments and numerical modeling of sand movement under compound waves are required for better understanding sand transport due to three-dimensional waves.

The objectives of the present study are to describe sand transport mechanism under three-dimensional compound waves through laboratory experiments and to develop a numerical model to estimate the net sand transport rate under compound waves. As a simple example of compound wave field, we selected the wave field in front of a breakwater with obliquely incident waves. This is because under such conditions the water particle near the bottom moves in various orbits, from linear to elliptic or circular orbit, so that they cover a wide range of conditions encountered in general compound wave conditions.

2. EXPERIMENTS

Experiments were performed in a 9m by 9m wave basin. A breakwater model was installed in the wave basin obliquely to the direction of wave incidence as shown in Fig. 1. The angle α between the breakwater and the incident wave was varied to 30, 45 and 60 degrees. All the bed in the wave basin was fixed except in a tray

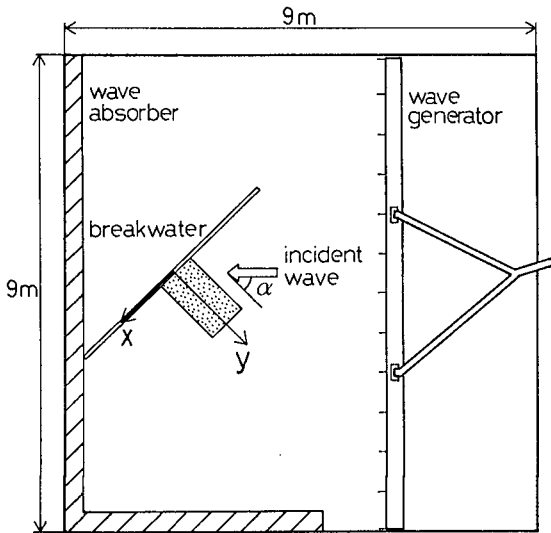


Fig. 1 Experimental setup.

installed in front of the breakwater. The tray was 120cm long, 40cm wide and 2cm deep. Well-sorted sand of median diameter $D = 0.16\text{mm}$ was filled in the tray to make an initially flat test bed. The depth in the wave basin was changed from 12 to 16cm. The period of incident waves was varied in a range from 0.65 to 1.41s. Thirty three runs of experiments were carried out for the condition of perfect reflection by changing the incident wave height so that experiments covered a wide range of conditions from weak sand movement to vigorous sand movement.

The reflection coefficient r of the breakwater was adjusted by changing the height of the top of the breakwater. Seventeen runs of experiments were performed for the condition of partial reflection by using a submerged breakwater model. The total number of experimental runs was 50.

The distribution of wave height was measured by capacitance-type wave gages. The variation of near-bottom velocities was measured by using a two-component electro-magnetic current meter. The sensor of the current meter shaped a cylinder of 1cm in diameter. The data were recorded on a magnetic tape through a personal computer system.

The development of sand ripples and the change of bottom profile in the test bed was measured in detail by vertically inserting a transparent film coated with grease oil. The sand surface level as well as the sand ripple geometry were evaluated from the trace of sand particles attached to the transparent film.

The test bed was divided into twelve parts and the sand in each part was collected separately after each run of experiments. The volume of sand was measured by using a mess-cylinder. The sand was repeatedly thrusted by a stick until it reached densely packed condition. The distribution of net sand transport rates in x (parallel to the breakwater) and y (perpendicular to the breakwater) directions were evaluated from the amount of the collected sand.

3. RESULTS OF EXPERIMENTS

3.1 Wave field and near-bottom velocities in front of a breakwater

Figure 2 shows an example of wave height distribution, bottom profile and net sand transport rates measured in front of a breakwater. The wave field was found to be calculated in a good accuracy by a third-order nonlinear wave theory (solid line) derived by Hsu *et al.* (1978). The net sand transport rate q_x parallel to the breakwater was found to be positive at nodes and negative at loops, which was also the case in most of the experimental runs.

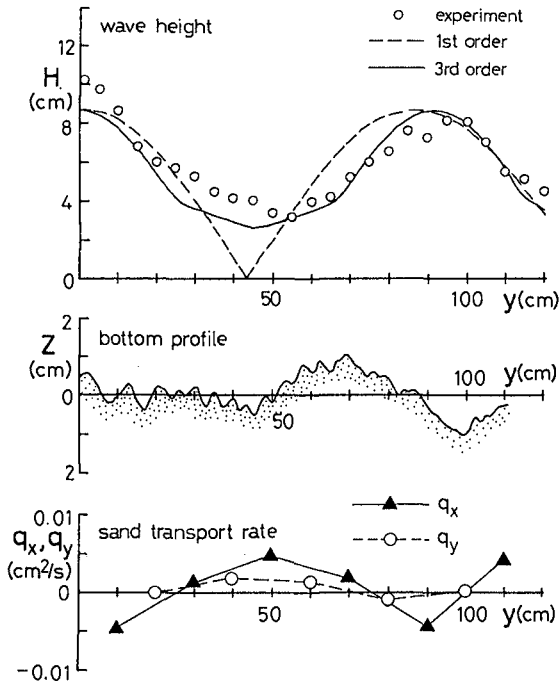


Fig. 2 Distributions of wave height, bottom profiles and net sand transport rates.

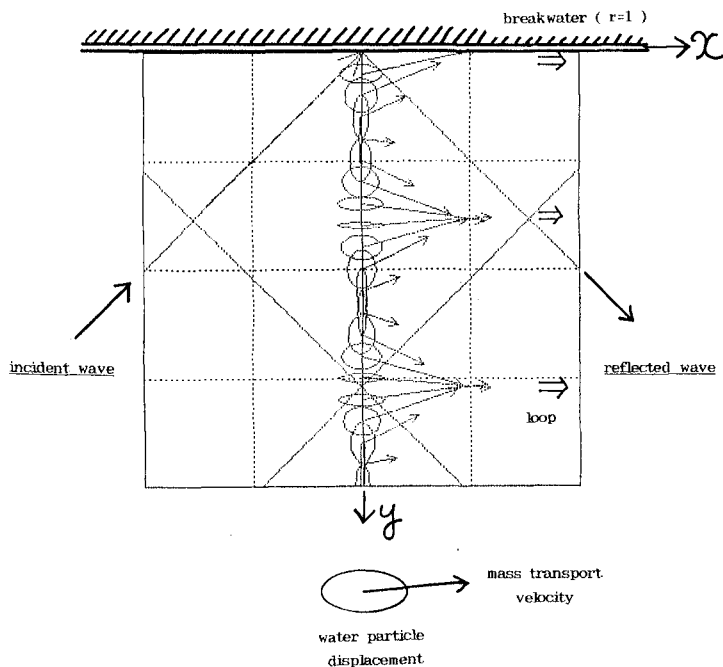


Fig. 3 Near-bottom velocity field in front of a breakwater.

Figure 3 shows the orbital motion due to waves as well as mass transport velocity in front of the breakwater with perfect reflection. The water particle near the bottom moves in circular, elliptic and linear orbit dependent on the distance from the breakwater. The nonlinear theory predicts that the wave orbital velocity becomes asymmetric in such a way that the velocity under wave crest is larger than that under wave trough. Measurements with an electro-magnetic current meter and dye injection supported the validity of the third-order wave theory in the estimation of the wave induced orbital velocity and the mass transport velocity.

3.2 Sand ripple geometry

Figure 4 shows sand ripple pattern observed in front of a breakwater. Three types of sand ripples were observed, that is, two-dimensional (2-D) ripples parallel to the breakwater, brick pattern ripples and 2-D ripples perpendicular to the breakwater.

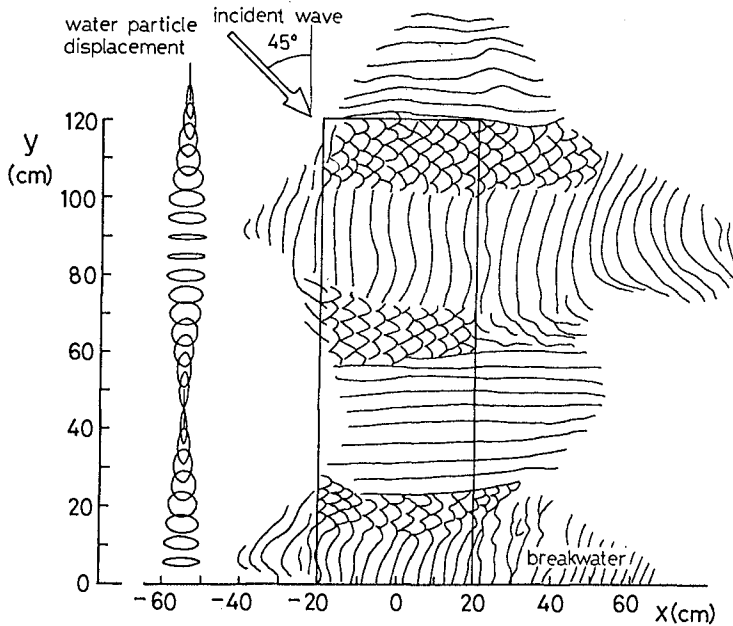


Fig. 4 Sand ripple pattern observed in front of a breakwater.

Figure 5 shows the classification of ripple patterns in terms of the Shields parameter Ψ and d_{oy}/d_{ox} , where d_{ox} and d_{oy} are diameters of water particle displacement in x and y directions. The Shields parameter was expressed by

$$\Psi = \frac{f_w u_m^2}{2sgD} \quad (1)$$

where $s(=1.65)$ was the specific gravity of sand particle in water, g the gravity acceleration, f_w the friction factor and u_m the maximum velocity near the bottom. The friction factor was estimated by using Jonsson's formula in terms of the maximum velocity and the diameter of near-bottom water particle displacement. The roughness element was assumed to be the diameter of the sand particle.

It was found that brick pattern ripples developed in the range

$$0.5 < d_{oy}/d_{ox} < 2 \quad (2)$$

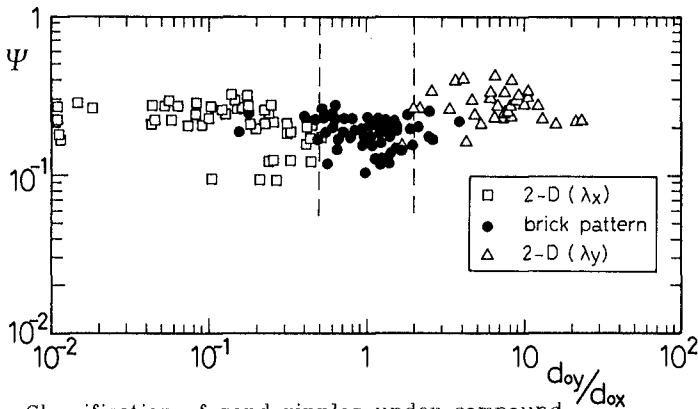


Fig. 5 Classification of sand ripples under compound waves.

and two-dimensional ripples developed for

$$d_{oy} / d_{ox} < 0.5 \text{ and } d_{oy} / d_{ox} > 2 \quad (3)$$

It was also found that the wavelength and wave height of sand ripples were able to be evaluated in terms of d_{ox} , d_{oy} and Ψ . The wavelengths λ_x and λ_y of sand ripples were found to be estimated by

$$\begin{aligned} \lambda_x &= 0.6 d_{ox} \\ \lambda_y &= 0.6 d_{oy} \end{aligned} \quad (4)$$

for both 2-D and brick pattern ripples. The ripple wave steepness was predicted by

$$\eta / \lambda = 0.15 \quad (5)$$

for 2-D ripples and

$$\eta / \lambda = 0.11 \quad (6)$$

for brick pattern ripples. These equations will be used in the numerical model to estimate sand ripple geometry.

3.3 Sand movement mechanism

Significant sand suspension was observed in most of experimental runs. The suspended sand concentration was observed to be determined by the asymmetry in the near-bottom velocity variation. The concentration was high under wave crests and low under wave trough since the velocity magnitude under wave crests was larger than that under wave trough in nonlinear wave field. The net direction of sand transport was determined by the balance between the transport due to the asymmetry in velocity variation and that due to the mass transport velocity.

Sand suspension was not significant in the area where brick pattern ripples were developed. The reason for this was considered that the maximum velocity was in general small over brick pattern ripples and that a strong vortex which contains a large amount of sand was not developed efficiently on the lee side of brick pattern ripples.

4. NUMERICAL MODEL

4.1 Sand entrainment at the ripple crest

In order to estimate the sand transport rate under compound waves, a numerical model was developed which evaluated the net sand transport rate above rippled bed by using near-bottom velocities calculated by the nonlinear wave theory. The outline of the model is schematically shown in Fig. 6.

Nielsen (1986) proposed on the basis of laboratory experiments a relation between the temporally-averaged sand concentration C_o at the bottom and the Shields parameter by

$$C_o = 0.005 \Psi_r^3 \tag{7}$$

where Ψ_r was the Shields parameter corrected by the flow acceleration at the ripple crest defined by

$$\Psi_r = \Psi / (1 - \pi \eta / \lambda)^2 \tag{8}$$

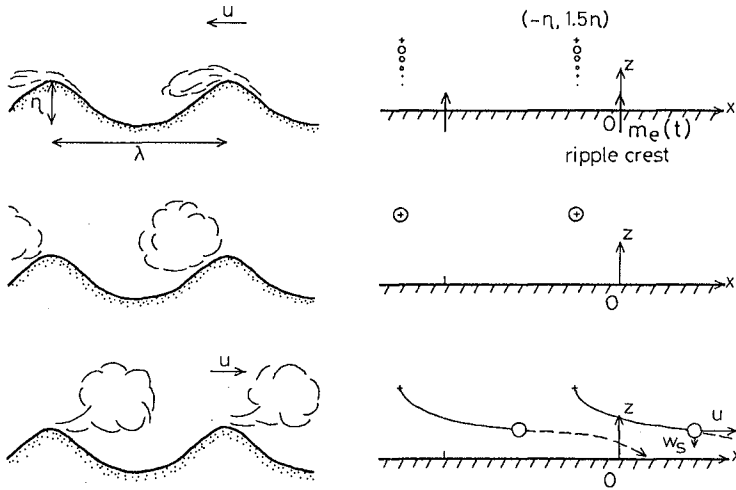


Fig. 6 Schematic diagram of the numerical model.

The rate $m_e(t)$ of the sand entrainment at ripple crests was assumed to be proportional to the third power of the instantaneous Shields parameter $\Psi_r(t)$ as,

$$m_e(t) = \alpha_c \Psi_r(t)^3 w_s \lambda \quad (9)$$

where w_s denotes the settling velocity of sand particles, λ the wavelength of ripples, α_c a nondimensional constant and $\Psi_r(t)$ was instantaneous Shields parameter at ripple crest defined by

$$\Psi_r(t) = \frac{f_w u(t)^2}{2sgD(1-\pi\eta/\lambda)^2} \quad (10)$$

The value of α_c was determined so that the entrainment during a period be the same as that estimated from the suspended sand concentration above rippled beds. According to Eq.(7) the amount M_s of sand entrained during one wave period over one wavelength of ripples was estimated by

$$M_s = 0.005 \Psi_r^3 w_s T \lambda \quad (11)$$

By assuming that the velocity variation is sinusoidal as a first approximation and that the total amount of entrainment was prescribed by Eq.(11), we can evaluate α_c in Eq.(9) as 0.016.

The numerical calculation was proceeded with a time step of $\Delta t = T/40$. On the rippled bed, sand was carried on the upstream slope of ripple crest and was thrown at the ripple crest into suspension. In order to simplify the complicated mechanics of sand movement on the ripple slope, an assumption was made in the present model that all the sand was entrained at the ripple crest. The amount m_s of sand entrained during each time step was given by

$$m_s = m_e(t) \Delta t \quad (12)$$

4.2 Transport of suspended sand particles

The entrained sand was assumed to be trapped in the vortex on the lee side of ripple crest and be transported after the flow direction changed. The movement of suspended sand cloud was numerically traced on the assumption that each sand cloud was transported with the same speed as the near-bottom water particle velocity due to wave orbital motion plus the Eulerian mass transport velocity. Net sand transport rates were evaluated from the settling position of the each sand cloud.

4.3 Application to the compound wave field

When we apply the model to compound wave fields, an assumption is needed on the position of suspended sand cloud formation. Figure 7 shows an example of water particle displacement at a node of obliquely incident standing waves. The water particle displacement

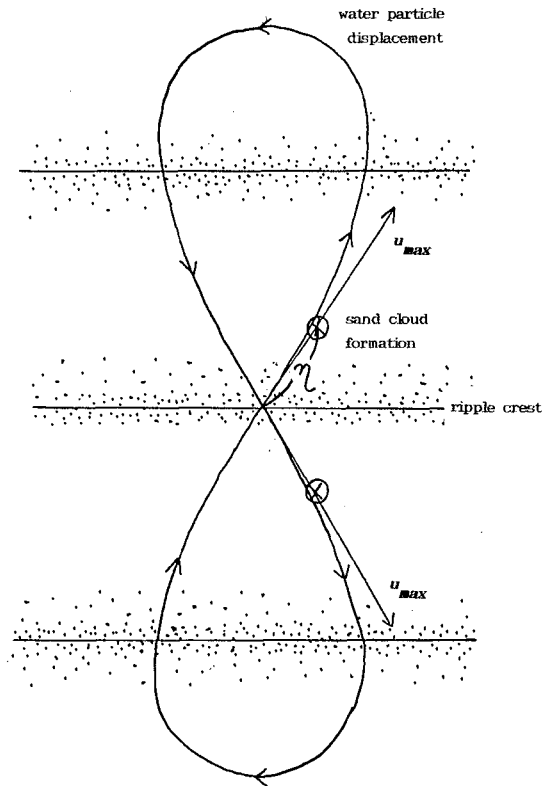


Fig. 7 Example of water particle displacement near the bottom.

was calculated by using the third order nonlinear theory. The figure illustrates that water particles near the bottom move in an 8-shaped orbit so that the velocity component v in the y direction is positive when the velocity is maximum. As sand moved most vigorously when the velocity was maximum, the most appropriate position would be the position on the lee side of ripple crest in the direction of the maximum velocity. The transport of sand cloud was calculated in the same manner as in the one-dimensional case.

4.4 Comparison with experiments

The applicability of the numerical model was examined by calculating the net sand transport rate under the following three-conditions; a finite-amplitude progressive wave, a standing wave and the compound wave field in front of a breakwater with oblique incidence.

Sato and Horikawa (1986) carried out movable bed experiments in an oscillatory flow tunnel and measured net sand transport rates over sand ripples for the condition of asymmetric oscillatory flows. Velocity histories of the oscillatory flows were simulated by using the fifth-order Stokes and the third-order cnoidal wave theory. Figure 8 shows a comparison between net sand transport rates $|\Phi_c|$ calculated by the numerical model and those $|\Phi_m|$ measured by Sato and Horikawa (1986) for the condition of asymmetric oscillatory flows. It was confirmed that the present model was able to estimate the net sand transport rate for asymmetric oscillatory flows observed in shallow water progressive waves.

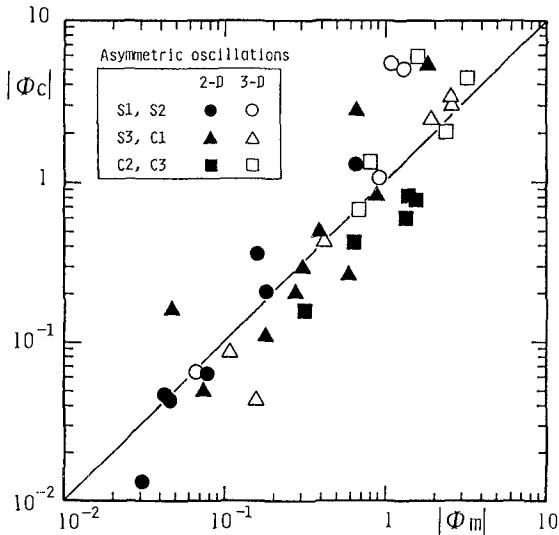


Fig. 8 Comparison of net sand transport rate for asymmetric oscillatory flows.

Irie and Nadaoka (1984) classified the seabed scour pattern under standing waves into two types. They defined L-type movement in which bed materials move from nodes to loops and N-type movement in which bed materials move from loops to nodes. Based on laboratory experiments, they concluded that the occurrence of the two types depended on the Ursell number of the incident wave and the ratio of near-bottom velocity amplitude to the settling velocity of sand particles.

The present model was applied to the condition of standing wave with normal incidence. The condition of calculation was varied systematically in a range with the water depth 8-30cm, the incident wave height 2-10cm, the wave period 0.8-2s and the sediment

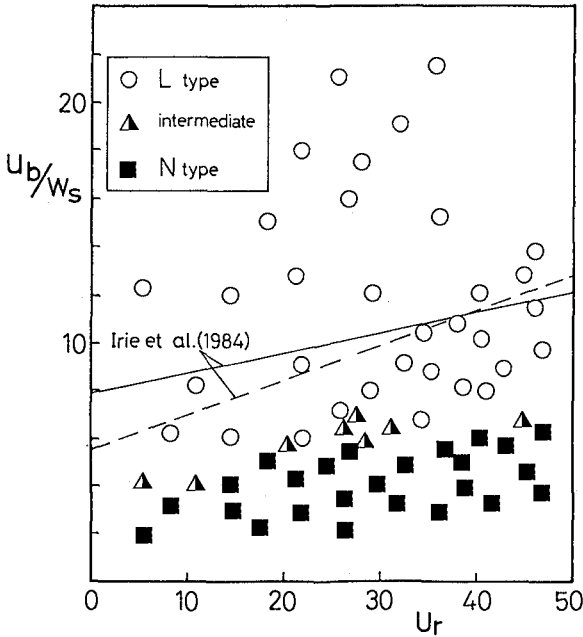


Fig. 9 Classification of sea bed scour under standing wave.

diameter 0.1-0.5mm. Figure 9 shows the occurrence of N- and L-type movement in the numerical calculation. The symbol \circ indicates the L-type movement and \blacksquare indicates the N-type movement. The solid line indicates the criterion empirically proposed by Irie and Nadaoka (1984) on the basis of laboratory movable bed condition and the broken line indicates that judged from the movement of sand particles distributed on a fixed bed. Although the model tends to produce L-type movement even for smaller values of u_b/w_s , the numerical model reproduces the tendency that the bed type changes from N-type to L-type with the increase of u_b/w_s .

Figure 10 shows a comparison of net sand transport rates under compound waves. The agreement between the experimental data and the calculation supports the applicability of the present model to the sand transport under compound waves.

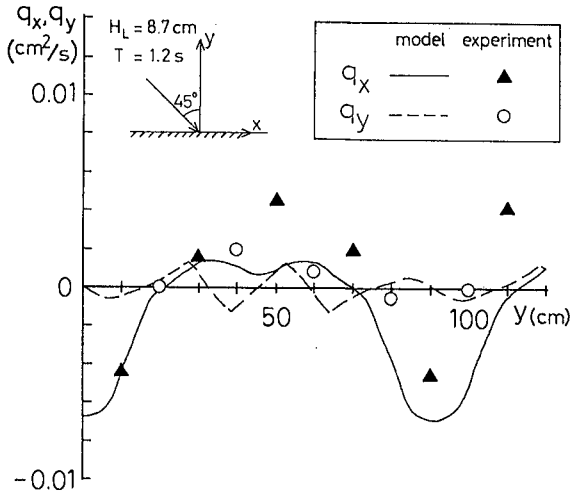


Fig. 10 Comparison of net sand transport rate for obliquely incident waves.

5. CONCLUSIONS

Characteristics of sand movement under compound waves were described through laboratory experiments. A numerical model of sand transport due to compound waves was presented which involved the process of sand suspension above rippled beds. The applicability of the model to a variety of conditions was confirmed with experimental data. As the model requires only the velocity variation near the bottom, it will be easy to apply the model to three-dimensional directional waves.

6. REFERENCES

- Hsu, J. R. C., Y. Tsuchiya and R. Silvester (1979): Third-order approximation to short-crested waves, *J. Fluid Mech.*, Vol. 90, pp. 179-196.
- Sato, S. and K. Horikawa (1986): Laboratory study on sand transport over ripples due to asymmetric oscillatory flows, *Proc. 20th Conf. on Coastal Eng.*, pp. 1481-1495.
- Irie, I. and K. Nadaoka (1984): Laboratory reproduction of seabed scour in front of breakwaters, *Proc. 19th Conf. on Coastal Eng.*, pp. 1715-1731.
- Hsu, J. R. C., R. Silvester and Y. Tsuchiya (1980): Boundary-layer

velocities and mass transport in short-crested waves, *J. Fluid Mech.*, Vol.99, part 2, pp.321-342.

Nielsen, P. (1986): Suspended sediment concentrations under waves, *Coastal Eng.*, Vol.10, pp.23-31.

Silvester, R. (1986): The influence of oblique reflection on breakwaters, *Proc. 20th Conf. on Coastal Eng.*, pp. 2253-2267.